

Self-aligned silicon fins in metallic slits as a platform for planar wavelength-selective nanoscale resonant photodetectors

Krishna C. Balram* and David A. B. Miller

Department of Electrical Engineering, Edward L. Ginzton Laboratory, Stanford University, California 94305, USA
*kcbalram@stanford.edu

Abstract: We propose and demonstrate a novel nanoscale resonant metal-semiconductor-metal (MSM) photodetector structure based on silicon fins self-aligned to metallic slits. This geometry allows the center wavelength of the photodetector's spectral response to be controlled by the silicon fin width, allowing multiple detectors, each sensitive to a different wavelength, to be fabricated in a single-step process. In addition, the detectors are highly efficient with simulations showing ~67% of the light ($\lambda = 800$ nm) incident on the silicon fin being absorbed in a region of thickness ~170 nm whereas the absorption length at the same wavelength is ~10 μm . This approach is promising for the development of multispectral imaging sensors and low-capacitance photodetectors for short-range optical interconnects.

©2012 Optical Society of America

OCIS codes: (110.4234) Multispectral and hyperspectral Imaging; (350.4238) Nanophotonics and photonic crystals; (250.5403) Plasmonics; (070.5753) Resonators; (230.5160) Photodetectors; (200.4650) Optical interconnects; (300.0300) Spectroscopy.

References and links

1. G. Themelis, J. S. Yoo, and V. Ntziachristos, "Multispectral imaging using multiple-bandpass filters," *Opt. Lett.* **33**(9), 1023–1025 (2008).
2. A. F. H. Goetz, G. Vane, J. E. Solomon, and B. N. Rock, "Imaging spectrometry for earth remote sensing," *Science* **228**(4704), 1147–1153 (1985).
3. R. M. Levenson and J. R. Mansfield, "Multispectral imaging in biology and medicine: slices of life," *Cytometry A* **69A**(8), 748–758 (2006).
4. G. Minas, R. F. Wolffenbuttel, and J. H. Correia, "A lab-on-a-chip for spectrophotometric analysis of biological fluids," *Lab Chip* **5**(11), 1303–1309 (2005).
5. T. Ishi, J. Fujikata, K. Makita, T. Baba, and K. Ohashi, "Si nano-photodiode with a surface plasmon antenna," *Jpn. J. Appl. Phys.* **44**(12), L364–L366 (2005).
6. L. Tang, S. E. Kocabas, S. Latif, A. K. Okyay, D.-S. Ly-Gagnon, K. C. Saraswat, and D. A. B. Miller, "Nanometre-scale germanium photodetector enhanced by a near-infrared dipole antenna," *Nat. Photonics* **2**(4), 226–229 (2008).
7. D.-S. Ly-Gagnon, K. C. Balram, J. S. White, P. Wahl, M. L. Brongersma, and D. A. B. Miller, "Routing and photodetection in subwavelength plasmonic slot waveguides," *Nanophotonics* **1**, 9–16 (2012).
8. T. Tanemura, K. C. Balram, D.-S. Ly-Gagnon, P. Wahl, J. S. White, M. L. Brongersma, and D. A. B. Miller, "Multiple-wavelength focusing of surface plasmons with a nonperiodic nanoslit coupler," *Nano Lett.* **11**(7), 2693–2698 (2011).
9. E. Laux, C. Genet, T. Skauli, and T. W. Ebbesen, "Plasmonic photon sorters for spectral and polarimetric imaging," *Nat. Photonics* **2**(3), 161–164 (2008).
10. S. Y. Chou and M. Y. Liu, "Nanoscale tera-hertz metal-semiconductor-metal photodetectors," *IEEE JQE* **28**(10), 2358–2368 (1992).
11. P. Neutens, P. Van Dorpe, I. De Vlainck, L. Lagae, and G. Borghs, "Electrical detection of confined gap plasmons in metal-insulator-metal waveguides," *Nat. Photonics* **3**(5), 283–286 (2009).
12. R. J. Walters, R. V. A. van Loon, I. Brunets, J. Schmitz, and A. Polman, "A silicon-based electrical source of surface plasmon polaritons," *Nat. Mater.* **9**(1), 21–25 (2010).
13. D. Hisamoto, W.-C. Lee, J. Kedzierski, H. Takeuchi, K. Asano, C. Kuo, E. Anderson, T.-J. King, J. Bokor, and C. Hu, "FinFET-a self-aligned double-gate MOSFET scalable to 20 nm," *IEEE TED* **47**(12), 2320–2325 (2000).
14. D. A. B. Miller, "Device requirements for optical interconnects to silicon chips," *Proc. IEEE* **97**(7), 1166–1185 (2009).

15. J. H. Correia, G. de Graaf, S. H. Kong, M. Bartek, and R. F. Wolffenbuttel, "Single-chip CMOS optical microspectrometer," *Sens. and Act. A* **82**(1-3), 191–197 (2000).
 16. S. S. Wang and R. Magnusson, "Theory and applications of guided-mode resonance filters," *Appl. Opt.* **32**(14), 2606–2613 (1993).
 17. S. Johnson, S. Fan, P. Villeneuve, J. Joannopoulos, and L. Kolodziejski, "Guided modes in photonic crystal slabs," *Phys. Rev. B* **60**(8), 5751–5758 (1999).
 18. L. Cao, J. S. White, J.-S. Park, J. A. Schuller, B. M. Clemens, and M. L. Brongersma, "Engineering light absorption in semiconductor nanowire devices," *Nat. Mater.* **8**(8), 643–647 (2009).
 19. J. S. White, G. Veronis, Z. Yu, E. S. Barnard, A. Chandran, S. Fan, and M. L. Brongersma, "Extraordinary optical absorption through subwavelength slits," *Opt. Lett.* **34**(5), 686–688 (2009).
-

Introduction

If we could fabricate multiple nanoscale photodetectors with separately engineered wavelength sensitivities in a single step planar fabrication process, then we would enable many different applications. Primary among these are the development of multispectral image sensors [1] spanning the visible and near-IR spectral regions with applications ranging from remote sensing [2] to biology [3], next-generation color filter arrays for digital cameras where each pixel can be designed as a miniature visible spectrometer for accurate color reproduction and compact on-chip spectroscopes for lab-on-a-chip systems [4]. Here we propose and demonstrate a novel planar approach for fabricating tunable resonator-photodetector combinations where the center wavelength of the photodetector's spectral response is controlled by a lateral dimension. This approach is also promising for designing efficient high-speed low-capacitance nanoscale photodetectors for short-haul data communications applications at 850 nm, a wavelength at which silicon is weakly absorbing.

The ability of metals to confine light has long been used to realize many different kinds of antenna structures [5] [6], waveguides [7] and wavelength splitters [8] [9] for nanoscale photodetectors. Metals are also routinely used as contacts for high speed MSM (Metal-Semiconductor-Metal) photodetectors [10]. One key idea presented here is that the same metallic structure can be used simultaneously for light confinement, wavelength tuning, and carrier extraction [11] [12]. This additional functionality leads to devices that cannot be realized by purely dielectric structures. Designing resonators that can be tuned by a single lateral dimension leads to a planar single step fabrication process, reducing complexity and leading to low capacitance devices with potentially very high operating speeds. In addition, with the semiconductor industry moving towards 3D FINFET-like device architectures [13], the structures here can be fabricated on the same process platform and promise tight integration between transistors and photodetectors for next generation on-chip optical interconnects [14].

Discussion

The simplest way to incorporate wavelength sensitivity, when shining light onto the top surface of a photodetector, is to add an optical filter such as a "vertical" Fabry-Perot resonator made from layers of dielectrics [15]. To detect N wavelengths, however, we need to fabricate N filters of different thicknesses. Such fabrication requires (at least) N masking steps for the N subsequent etches or depositions to set the different filter thicknesses. This process becomes cumbersome with increasing N . One possible approach to designing resonators for multiple wavelengths in a single layer is to incorporate guided resonance filters, either as subwavelength gratings [16] or photonic crystal slabs [17], which can be excited in such a surface-normal configuration. But the structure then typically has to be multiple wavelengths in size laterally and is not so attractive for dense integration.

Mie-like resonances were recently observed in semiconductor nanowires [18], where the resonance wavelength depended on the diameter of the nanowire. Following from this physical observation of resonances tuned by a lateral dimension, we investigated absorption resonances in silicon fin geometries having a rectangular cross-section as shown in Fig. 1. Such fin structures have the important feature that they can be reliably fabricated using

conventional CMOS processes, with many resulting possibilities for electrically contacting the structures to make photodetectors.

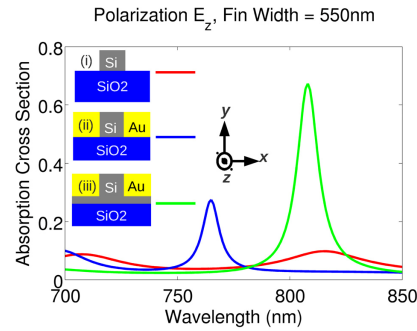


Fig. 1. Figure shows the simulated absorption cross-section for three devices (indicated in inset) to explain the origin of the device concept. Starting with a bare fin sitting on oxide [(i), red], both the Q-factor and the absorption cross-section can be increased by self-aligning a metallic slit [(ii), blue]. By leaving a thin base layer [(iii), green], we can extract photocurrent from the device and get additional responsivity by coupling to guided modes in the silicon base. The fin thickness in the simulations is 120 nm. For detailed device descriptions, see text.

In Fig. 1, we plot the spectra for the simulated absorption cross-section (defined as the fraction of the power incident on the silicon fin that is ultimately absorbed in the device) for three different device geometries. The simulations were performed using the RF module of the commercial finite element method solver COMSOL. The structures were excited by a plane wave with appropriate polarization (E_z or H_z) and the absorbed power was measured in a region defined by the silicon fin and a 1 μm wide silicon base region (an appropriate width given the possible depletion width for efficient photocarrier collection with the voltage bias used in the experiments). The absorbed power is calculated from a full field simulation of the device geometry in consideration under plane wave excitation and the incident power is calculated from a background simulation of a plane wave propagating in vacuum wherein the Poynting vector is integrated over a width equal to that of the silicon fin. In 2D, the absorption cross-section is a length and the fraction plotted in Fig. 1 should be interpreted as an “effective width” of the device. For example, the green curve in Fig. 1 plots the absorption cross section for the device geometry shown in Fig. 1(iii). At resonance, an absorption cross-section of 0.7 means that 70% of the light incident on the silicon fin is absorbed or the effective cross-sectional width of the device is $0.7 \times 550 \text{ nm}$ where 550 nm is the actual device width.

For a bare silicon fin of width 550 nm sitting on oxide [Fig. 1(i)] excited by a plane wave from air with polarization E_z , i.e., along the fin (red curve in Fig. 1), the absorption resonance is moderately broad (Q factor ~ 13) and the absorption cross-section is relatively small (~ 0.1) (though, because of this resonance, even this fractional absorption is much greater than we would expect for light shining on a silicon sheet of this same thickness at these wavelengths). If we self-align the silicon fin inside a metallic slit [Fig. 1(ii)], both the Q factor (~ 76) of the resonance (blue curve in Fig. 1) and the absorption cross-section (~ 0.27) show a marked increase.

To understand why this works, in Fig. 2(a) we show the electric field (E_z) inside the fin when the structure is excited by a plane wave with polarization E_z . We can see that the resonance is primarily due to the excitation of the fifth order transverse mode (having four nodes and fin width $\sim 5\lambda/2n_{\text{si}}$ where λ is the free space wavelength and n_{si} is the silicon refractive index) which can be thought of as a lateral standing wave set up between the fin sidewalls. The Q is improved primarily because the reflectivity off the sidewalls is enhanced by the presence of the metallic surfaces; note that the Fresnel intensity reflection coefficient at 850 nm wavelength (at normal incidence) for a silicon-air interface is 0.33 whereas that of a

silicon-gold interface is 0.93, so relatively much larger amounts of light would leak out of the side walls of the bare silicon fin of Fig. 1(i). The reasons for choosing to work with the fifth order resonance as opposed to say the 1st, 3rd or 7th are detailed in the appendix.

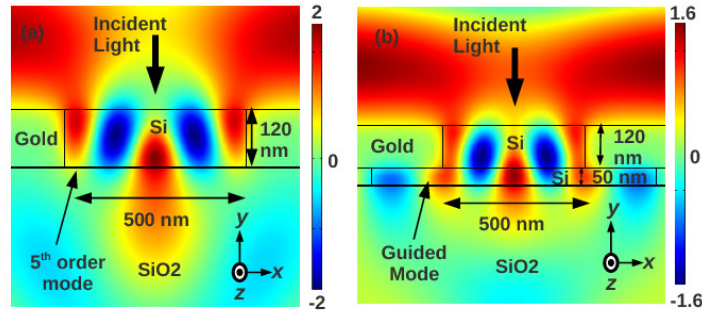


Fig. 2. (a) Figure shows the electric field (E_z) profile for a silicon fin ($w = 500\text{nm}$) self-aligned with a metallic slit under plane wave excitation at resonance ($\lambda = 721\text{nm}$). The field profile indicates that the absorption resonance corresponds to the excitation of the fifth order mode ($w \sim 5\lambda/2n_{\text{si}}$) in the silicon fin. (b) Figure shows the electric field profile (E_z) for a silicon fin of width 500 nm with a 50 nm silicon base layer under plane wave excitation at resonance ($\lambda = 767\text{nm}$). The excitation of guided modes in the silicon base layer, which leads to increased responsivity, can be seen.

To extract photocurrent from the structure, we leave a thin silicon base layer [Fig. 1(iii)]. The composite structure can be thought of as a cavity coupled to two waveguides at the bottom. Figure 2(b) shows the electric field (E_z) in the device under plane wave excitation, clearly showing the propagating modes excited in the silicon base layer. The silicon base layer acts as a waveguide clad by oxide at the bottom and gold at the top. The coupling of light into these horizontal waveguides provides additional loss channels for the resonator, lowering the Q factor (~ 67) of the resonance (green curve in Fig. 1) but increasing the absorption cross-section (0.67), and thus the responsivity, significantly. The guiding in the silicon base layer allows us the future possibility of engineering coupling between adjacent fins; such coupling is promising for the design of devices with greater functionality, such as more sophisticated spectral response.

The resonant width w for a given wavelength λ is roughly $w \sim 5\lambda/2n_{\text{si}}$. Figure 3(a) shows the calculated absorption cross-section for devices with three different widths (500 , 550 and 600 nm respectively), showing shift to longer wavelength with increasing width as expected. For $w = 550\text{ nm}$ (blue curve), the calculations show that 67% of the light incident on the slit width (at the resonant wavelength near $\sim 800\text{ nm}$) is absorbed in the silicon fin (thickness $\sim 120\text{ nm}$) and a depletion layer of $1\text{ }\mu\text{m}$ presumed width in the 50 nm thick silicon base region. This simulation shows that, in addition to controlling spectral response, this approach allows even this thin (170 nm) silicon layer to be an efficient photodetector at the $\sim 800\text{ nm}$ wavelength operating region of many short-distance optical links, a region where bare silicon has an absorption length of $\sim 10\text{ }\mu\text{m}$. Such an approach is particularly promising for high-efficiency low-capacitance photodetectors completely compatible with silicon CMOS processing on, for example, SOI wafers.

The simulations normalize the input power to the width of the silicon fin. When building pixel arrays, the issue of fill factor becomes important. Preliminary simulations have shown that fins with different widths (and thus different resonances) can be put as close as 150 nm to each other without significantly affecting their individual resonances.

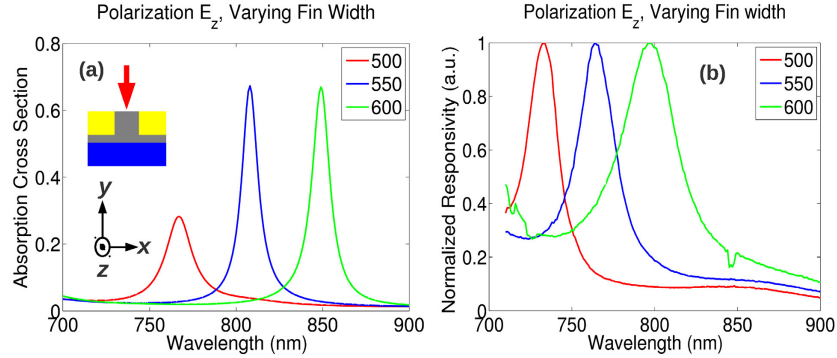


Fig. 3. (a) Figure shows the simulated absorption cross-section (as a fraction of device width), for three devices with fin widths of 500, 550 and 600 nm respectively, under plane wave excitation with polarization E_z . (b) Figure shows the measured absorption spectra for device with three different fin widths (500, 550 and 600 nm respectively). The spectra have been scaled to lie between 0 and 1.

Experimental results

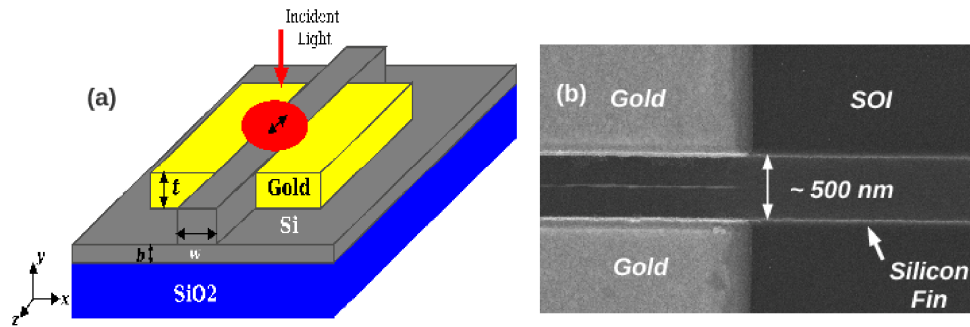


Fig. 4. (a) Figure shows the schematic of our structure. The absorption resonance in the structure can be tuned by varying the width of the structure w (for a given thickness t). A thin base region of thickness b is left to get reliable contacts to the structure and extract photocurrent. (b) Figure shows an SEM image of a representative device with width 500 nm and length 25 μm .

Figure 4(a) shows the device schematic. Figure 4(b) shows an SEM image of a representative device. The process starts with a silicon-on-insulator (SOI) wafer, which is oxidized and thinned to get the desired silicon device layer thickness (170 nm). The top thermal oxide is used as a hard mask for patterning the silicon fin using electron-beam lithography and dry etching (Reactive Ion Etching {RIE} using CHF_3/O_2 chemistry). The silicon fin thickness is controlled by measuring the silicon base thickness using ellipsometry (silicon device layer thickness = fin thickness + base thickness). Cr (2.5 nm) /Au contacts are then evaporated. The metal thickness is measured in situ during evaporation and is controlled to match the thickness of the silicon fin. The hard mask is then lifted off using 20:1 BOE (Buffered Oxide Etch) solution to leave the silicon fin self-aligned to the metallic slit.

Light from a tunable Ti-Sapphire laser (Spectra-Physics MaiTai, mode-locked with pulse spectral width of ~ 6 nm at 800 nm) is focused on the sample using a Mitutoyo Achromat Objective (20x, NIR) with a spot size ~ 2.5 μm (FWHM intensity diameter). The polarization is controlled using a Glan-Laser polarizer and a broadband halfwave plate (Fresnel Rhomb). The sample is biased by applying a voltage (~ 250 mV) on the two gold pads using a parameter analyzer and the photocurrent is detected by a lock-in amplifier which is phase-locked to the reference from a mechanical chopper (frequency ~ 2 kHz) in the laser beam. The

normalization spectrum is measured at the location of the sample using a power meter (Thor Labs PM 700).

Figure 3(b) shows the measured responsivity for devices with three different widths (500, 550 and 600 nm) when excited with polarization parallel to the slit (E_z). To illustrate the peak shifts, the plots are scaled to lie between 0 and 1. The spectra show the same trends as the simulations of Fig. 3(a), which simulated the absorption in these devices. The reasonable agreement between simulation and measurement gives us confidence that these structures can be predictably designed for more complex responses.

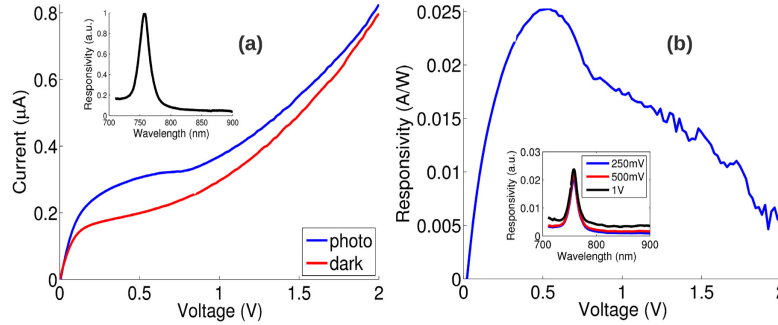


Fig. 5. (a) shows the I-V characteristic of a representative device ($w \sim 500\text{nm}$) in the dark and under laser excitation at resonance (the responsivity of the device is shown in the inset). (b) Figure shows the measured responsivity of the device as a function of the bias voltage. The absorption spectra for three different bias voltages are shown in the inset.

Figure 5(a) shows the I-V characteristic of a representative device ($w \sim 500\text{ nm}$) in the dark and under laser excitation (power $4.2\ \mu\text{W}$) at resonance (spectra inset). Figure 5(b) shows the responsivity (A/W) as a function of bias voltage. The reason for the drop in responsivity at higher bias is unclear. One possible mechanism could be build-up of charges at the silicon-oxide interface leading to electrostatic gating effects. Simulations (see Fig. 3(a)) predict $\sim 30\%$ of the light incident on the silicon fin would be absorbed in this device at resonance under plane wave illumination. Scaling to the fraction of the power incident on the fin with the actual incident laser spot of $\sim 2.5\ \mu\text{m}$ FWHM intensity diameter, and assuming perfect internal photocarrier collection efficiency, we would predict a responsivity of $0.06\ \text{A/W}$. The measured peak responsivity is $\sim 0.025\ \text{A/W}$, which is of the same magnitude as the predicted responsivity, but somewhat smaller. We note that the top surface and sidewalls of the silicon fin are not passivated, leading to possible surface recombination that could limit the internal photocarrier collection efficiency. Improved device design (e.g., using a pin detector as opposed to an MSM structure) and surface passivation could improve responsivity considerably.

When excited with polarization perpendicular to the slit (H_z), the structure also supports a plasmon resonance (Fig. 6(a)) which can be thought of as the vertical Fabry-Perot resonance of the MIM (Metal-Insulator-Metal) mode formed by the gold slit and the silicon fin [19], and we can observe this resonance experimentally. Unlike the dielectric resonance, which cuts off for small widths ($w < 5\lambda/2n_{\text{si}}$), the plasmon resonance persists down towards zero width, but it is not so easily tuned by lateral dimensions. Figure 6(b) shows the measured responsivity of a device showing both the dielectric and plasmon resonances.

For multispectral imaging sensors working with unpolarized light in applications like remote sensing, the polarization sensitive response of the device does reduce the responsivity. But given the fact that the size of the device is subwavelength, one can imagine fins with different orientations placed close together to compensate for the polarization sensitivity. In addition, the polarization response can be engineered by changing the geometry of the device which makes it attractive for polarization sensitive imaging applications.

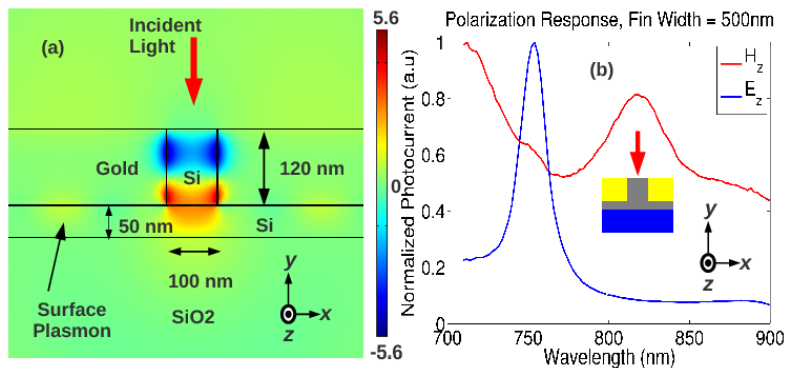


Fig. 6. (a) Figure shows the electric field (H_z) profile for a silicon fin ($w = 100$ nm) self-aligned with a metallic slit under plane wave excitation (b) Figure shows the measured normalized responsivity of a silicon fin of width 500 nm in two orthogonal polarizations.

Conclusions

In summary, we have demonstrated a novel self-aligned fabrication procedure for silicon fins inside metallic slits and have shown that this structure supports strong absorption resonances in polarizations parallel to and perpendicular to the slit. Additionally, we have demonstrated controlled tuning of the resonance by varying the width of the fin, allowing devices of different spectral sensitivity in a single planar process strongly compatible with CMOS processing, and permitting efficient photodetectors in thin Si structures even in spectral regions of weak Si optical absorption. We believe that these devices represent a significant step towards the development of detectors for multi-spectral imaging systems and on-chip optical interconnects

Appendix: Choice of the $5\lambda/2$ resonance

The proposed structure supports resonances at integral multiples of half-wavelength ($\lambda/2n_{\text{Si}}$, $3\lambda/2n_{\text{Si}}$ and so on). The reason we chose the $5\lambda/2n_{\text{Si}}$ resonance to work with is that it gives us the sharpest resonance with maximum absorption cross-section (which is critical for designing these resonator photodetector structures) while remaining below a free-space wavelength (which is crucial for dense integration). Figure 7(a) shows the simulated absorption cross-section (as a fraction of fin width) plotted against fin width (for a free-space wavelength $\lambda = 850$ nm). The plot indicates the fin widths corresponding to the first three lateral resonances of the structure, clearly showing that the $5\lambda/2$ resonance has the highest absorption cross-section. Figure 7(b) plots the absorption spectra for the first three lateral resonances, clearly showing that the $5\lambda/2$ resonance provides the sharpest Q, which is important when designing tunable resonator structures.

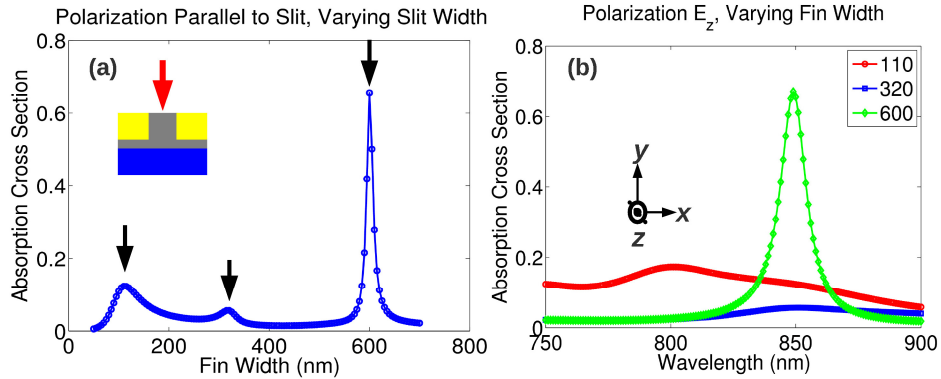


Fig. 7. (a) Figure shows the simulated absorption cross-section (as a fraction of fin-width) plotted against fin width at $\lambda = 850$ nm. The arrows indicate the locations of the $\lambda/2n_{\text{si}}$, $3\lambda/2n_{\text{si}}$ and $5\lambda/2n_{\text{si}}$ resonances respectively. (b) Figure shows the simulated absorption cross-section spectra (as a fraction of fin width) for the first (red), third (blue) and fifth (green) order lateral resonances. The 5th order resonance has both the highest Q (good for tuning the resonance with width) and the highest absorption cross-section (for making efficient detectors).

Acknowledgments

We would like to thank Dr. Takuo Tanemura for valuable discussions during the course of this work. Krishna C. Balram acknowledges the support of the ST Microelectronics Stanford Graduate Fellowship. This work is supported by the Interconnect Focus Center, one of the six research centers funded under the Focus Center Research Program, a Semiconductor Research Corporation program and by the and AFOSR Robust and Complex On-Chip Nanophotonics MURI. Work was performed in part at the Stanford Nanofabrication Facility (a member of the National Nanotechnology Infrastructure Network) which is supported by the National Science Foundation under Grant ECS-9731293.